SEMARAK ILMU PUBLISHING

Semarak Engineering Journal

Journal homepage:
https://semarakilmu.com.my/journals/index.php/sem_eng/index
ISSN: 3036-0145

Effect Of Nozzle Temperature on The Physical Properties of Inconel 718 Specimens Additively Manufactured by Fused Filament Fabrication

Nurainaa Mazlan[1], Nur Hidayah Musa[1], Shahir Mohd Yusuf[1,*], Nur Azmah Nordin[1], Saiful Amri Mazlan[1]

[1] Engineering Materials & Structures (eMast) iKohza, Malaysia-Japan International Institute of Technology (MJIIT), Universiti Teknologi Malaysia, 54100 Kuala Lumpur, Malaysia

ARTICLE INFO

Article history:
Received 2 February 2024
Received in revised form 15 March 2024
Accepted 27 April 2024
Available online 30 May 2024

Keywords:
Additive manufacturing; fused filament fabrication; metallic materials; Inconel 718; nozzle temperature; properties

ABSTRACT

In this study, the effect of nozzle temperature, (T_n) (varied between 200°C and 300°C) during the printing stage on the relative density, hardness, and porosity of sintered Inconel 718 (IN 718) specimens are investigated for the first time. The results show a general trend of increasing relative density and hardness values, as well as reduced porosity with an increase in T_n values. The highest relative density (92.34%), hardness (188 HV) and lowest porosity (7.66%) are all achieved at T_n=290°C. The outcomes of this study establish the profound impact of adjusting processing parameters even at the initial printing stage towards the properties of the sintered parts.

1. Introduction

Inconel 718 (IN718) is a widely used nickel-base superalloy that serves as an important material in the aeronautical, aerospace, and nuclear industries due to its high strength and exceptional oxidation and corrosion resistance at elevated temperatures [1,2]. The strength of this material is primarily contributed by the γ"-phase (Ni_3Nb) and some γ', δ, and carbides, while its oxidation and corrosion resistances result from the high Cr content (17-21%) [3].

In the past 10 – 15 years, additive manufacturing (AM), or more commonly known as 3D printing has shown significant promise to fabricate metallic parts with complex geometries and intricate features via a layer-wise manufacturing approach, thereby reducing material waste and lead time [4-7]. In particular, powder bed fusion (PBF) and directed energy deposition (DED) are the two most common AM technologies that have shown significant promise in producing metallic components prototypes and end-applications [8]. Both PBF and DED processes use high-energy laser/electron beam to selectively melt and fuse metallic powders (PBF and DED) or wires (DED only) and form the desired 3D shape pre-designed in computer aided design (CAD) software. However, PBF and DED operations require high investment costs due to the use of high-power heat sources, as well as the complex and proprietary nature of the required equipment [9,10]. Therefore, researchers have been

* *Corresponding author.*
E-mail address: shahiryasin@utm.my

exploring affordable alternatives for producing metallic components using AM technology, such as fused filament fabrication [11].

Recently, fused filament fabrication (FFF), an AM process within the material extrusion (ME) category has emerged as a viable low-cost AM approach to produce metallic parts, following a 3-step printing-debinding-sintering process derived from conventional metal injection molding (MIM) and powder metallurgy (PM) techniques [12]. Firstly, green parts are fabricated by extruding melted metal-polymer filament feedstock through one or more heated nozzles, often ranging between 200°C – 300°C. The use of metal-polymer filaments, typically composed of metal powders (50-65%) bound together with a polymer binder system (35-50%) is crucial since direct extrusion of the melted metal only is impossible due to the steep melting point of most metals/alloys, often reaching >1000°C that cannot be catered to by any presently available nozzles for FFF printers [13-15]. Therefore, debinding and sintering of the as-printed (green) parts are necessary to obtain fully consolidated metal parts, such that debinding completely eliminates the polymer binder, whereas sintering fuses the metallic particles to form fully dense metallic specimens [16]. So far, numerous studies have been dedicated to investigating the effect of post-printing measures such as sintering parameters and other heat treatment procedures on the microstructures and properties of metal FFF parts [17-21].

However, not many studies have focused on the influence of adjusting processing parameters during the initial printing stage on the properties of sintered metal FFF parts to the best of our knowledge. So far, only flow rate multiplier, layer thickness, print speed, and extrusion temperature have been investigated in FFF printing of 17-4PH SS by Godec *et al.,* [12] and Gonzalez-Gutierez *et al.,* [22]. However, no correlations between the manipulation of these parameters on the density, porosity, and hardness of the sintered parts are provided in these studies. Therefore, this study aims to address this gap by investigating the effect of nozzle temperatures (T_n) on the physical properties of FFF-3D printed IN718 specimens after sintering, including relative density, hardness, and porosity. The values of T_n varied from 200°C – 300°C during the printing process, followed by debinding and sintering processes. The relative density and Vickers microhardness measurements, as well as porosity analysis of the sintered specimens, are conducted to establish the inter-correlation among the nozzle temperature during printing and the physical properties of the sintered specimens.

2. Materials and Methods

2.1 Material and Specimen Preparation

A 3D printing filament comprising of IN718 powder particles (86 wt.%) and polylactic acid (PLA) polymer binder (14 wt.%) having a diameter of 1.75 mm is purchased from The Virtual Foundry (TVF), United States. The chemical composition of the filament as obtained from the supplier in wt.% is as follows: Ni (55.98%), Cr (17.10%), Fe (14.51%), Nb (5.72%), Mo (3.46%), Ti (0.81%), others (<0.1). A low-cost desktop FFF 3D printer, Creality CR-5 Pro is used to print 20mm^3 cubes via filament deposition through a heated hardened steel nozzle (0.6 mm diameter). The nozzle temperatures (T_n) are varied from 200°C to 300°C, while other parameters are kept constant: bed temperature: 60°C, infill flow rate: 100%, layer height: 0.2 mm, and nozzle speed: 80 mm/s. Subsequent one-step thermal debinding, followed by sintering processes are carried out continuously in an LH 30/14 Nabertherm GmbH electrical chamber furnace under atmospheric conditions. The debinding and sintering temperatures used in this study are 427°C (held for 2h) and 1260°C (held for 4h), respectively, based on the recommendations by TVF. The densification level of the sintered specimens is evaluated through the relative density, RD calculated by using the formula

$$\mathrm{RD} = \frac{\varrho_s}{\varrho_t} \mathrm{x}\ 100 \quad (1)$$

where ϱ_s is the specimen density, measured using the Archimedes method (ISO 2738), and ϱ_t is the theoretical density of IN718, 8.19 g/cm^3 [23]. Subsequently, the sintered specimens are ground and polished down to 1µm before proceeding with Vickers microhardness (HV) measurements and porosity characterizations. The HV values of the sintered specimens are measured using a Vickers microhardness test machine (HMV-G Series) with a load and holding time of 100 gf and 10 seconds, respectively. The HV values are averaged from 10 measurements throughout the surface of each specimen. The porosity content is quantified by using the formula

$$\text{Porosity (Pt)} = \left(1 - \left(\frac{\varrho_s}{\varrho_t}\right)\right) \times 100 \quad (2)$$

Meanwhile, the pore morphologies are determined through OM observations, and the pore sizes are determined by using the binarization procedure in ImageJ software based on the OM images [24].

3. Results and Discussion

IN718 cube specimens (green parts) are successfully fabricated within the range of T_n: 210°C – 290°C. However, T_n = 200°C is insufficient to melt the filament, whereas excessive filament melting at T_n = 300°C caused the nozzle to be clogged, resulting in printing failure for both cases.

The average RD (%) and HV values of the sintered specimens are shown in Table 1. A generally increasing trend of relative density and hardness is observed with increasing T_n values from 210°C – 290°. Interestingly, both RD and HV values experience a slight but not significant decrease at T_n = 270°C. Nevertheless, T_n = 290°C yields the highest relative density (92.34%) and hardness (188 HV) for the sintered specimens with the lowest porosity content (7.66%).

Table 1
Average relative density, hardness, and porosity of sintered specimens subjected to different nozzle temperatures

Nozzle temperature (°C)	Relative density, RD (%)	Vickers microhardness (HV)	Porosity (%)
210	66.81 ± 2	122 ± 17	33.19
230	70.39 ± 3	135 ± 21	29.61
250	71.97 ± 4	146 ± 35	28.03
270	68.74 ± 3	132 ± 26	31.26
290	92.34 ± 1	188 ± 14	7.66

The general improvement in RD with increasing T_n is likely caused by the enhanced material fluidity achieved at higher T_n values (up to 290°C in this study) that lowers the viscosity of the melted filament, which subsequently reduces the flow resistance to enable more matrix particles passing through the nozzle [12]. This results in enhanced filament melting and improved coalescence between the individual layers and strands of the melted filament [22]. Consequently, better compaction and packing density among the matrix particles is attained, thereby promoting neck formation and growth, as well as pore filling through diffusion during the sintering process that leads to improved densification levels [25,26]. Moreover, it is also clear that the HV variation of the sintered specimens follows that of the RD values, whereby increasing the T_n from 210°C to 290°C improves the HV value from 122 HV to 188 HV, which can be attributed to the similar aforementioned reasons [25].

Meanwhile, OM images displayed in Figure 1 clearly show the presence of irregular-shaped pores in all sintered specimens. However, qualitative observations suggest that the porosity content at increasing T_n values conforms to the trend of relative density and hardness variations shown in Table 1. At T_n = 210°C, the porosity size and content are measured as 11.58 µm and 33.19%, respectively. Upon increasing the value of T_n to 290°C, both quantities are significantly reduced to 4.18 µm and 7.66%, respectively. The formation of micron-sized pores in the metal FFF process is assumed to be similar to those observed in typical conventional sintering procedures due to the involvement of debinding and sintering stages after the initial printing of the green parts [10]. Nevertheless, the decreasing porosity content with increasing T_n values in this study can most likely be attributed to the enhanced diffusion of the sintering necks during the sintering process, owing to the improved compaction and packing density of the matrix particles at higher nozzle temperatures [25].

Finally, it is known that lower densification levels would increase porosity content and eventually decrease its hardness due to the pores being collapsed under load during the hardness test, thereby reducing the number of dislocations and grain boundaries that impede dislocation motions, and vice versa [27,28]. This is precisely being attained in the present study, whereby increasing T_n values generally improves the relative density and HV values, and reduces the porosity levels.

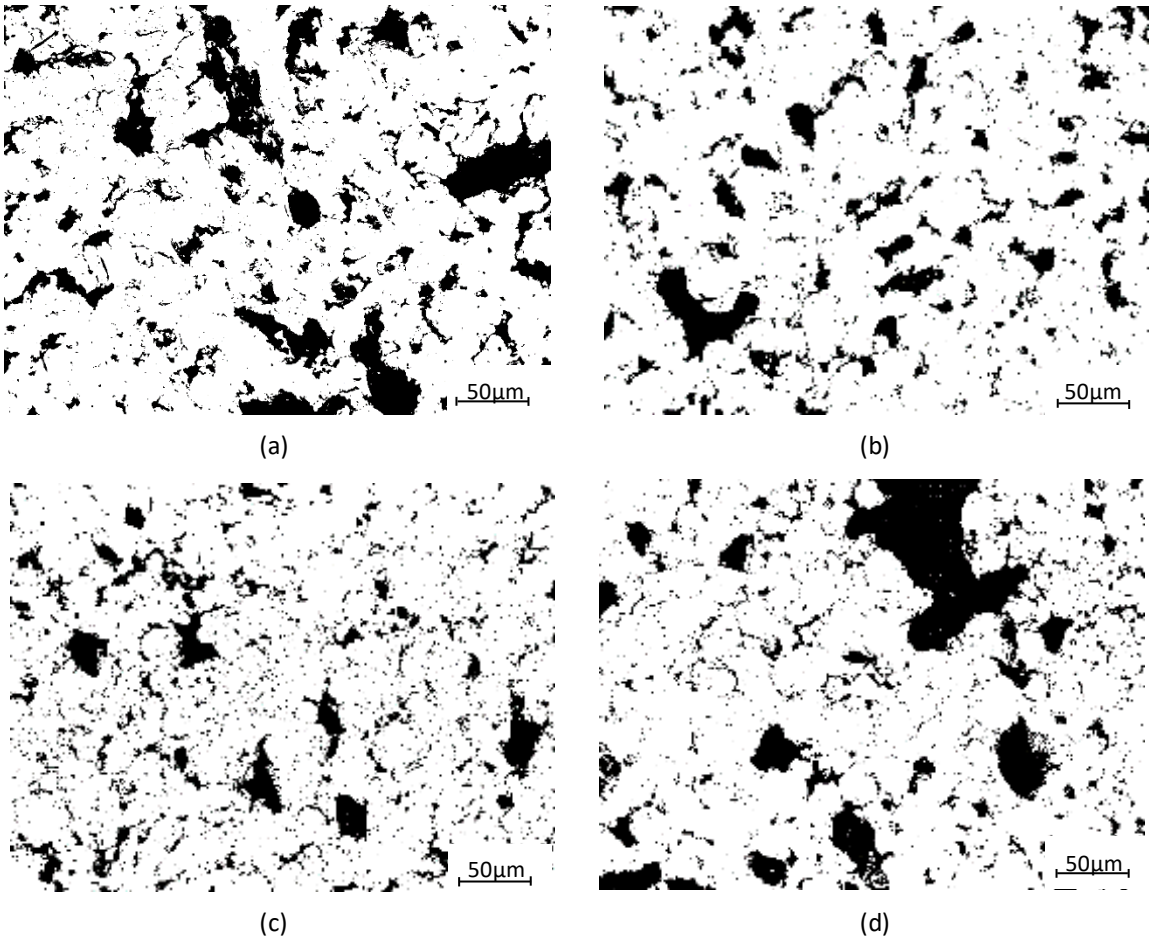

(a) (b)

(c) (d)

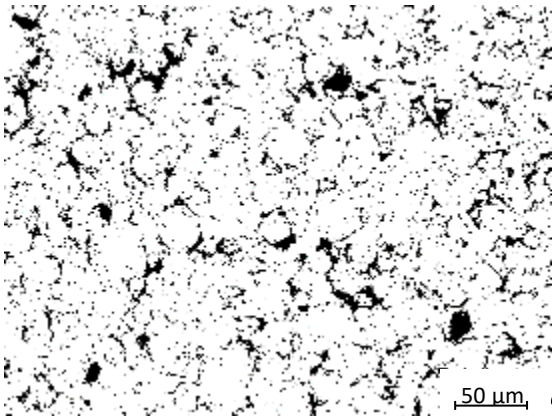

(e)

Fig. 1. OM images of IN718 sintered specimens at (a) T_n = 210°C, (b) T_n = 230°C, (c) T_n = 250°C, (d) T_n = 270°C, and (e) T_n = 290°C

4. Conclusions

This study investigates the effect of nozzle temperatures (T_n) during the initial printing stage on the physical properties (relative density, hardness, and porosity) of sintered IN718 specimens fabricated using the FFF AM technique through a 3-step printing-debinding-sintering stages. The findings from this study are summarized as follows:

i. IN 718 green specimens are successfully printed within the range of T_n values from 210°C to 290°C, whereas T_n = 200°C and T_n = 300°C result in printing failure.
ii. The highest relative density and hardness of 92.34% and 188HV, respectively with the lowest porosity content of 7.66% is obtained when the T_n is set to 290°C.
iii. Increasing T_n from 210°C to 290°C generally presents a positive trend for the relative density and hardness of the sintered specimens while reducing its porosity content through better material fluidity that improves the compaction and packing density of the matrix particles, which eventually enhances the diffusion of the sintering necks during the sintering stage.

Acknowledgements

This research was funded by the Ministry of Higher Education (MOHE) Malaysia through the Fundamental Research Grant Scheme (FRGS /1/2021/TK0/UTM/02/84).

References

[1] Youhua, Hu, Li Yimin, He Hao, Lou Jia, and Tang Xiao. "Preparation and mechanical properties of Inconel718 alloy by metal injection molding." *Rare Metal Materials and Engineering* 39, no. 5 (2010): 775-780. https://doi.org/10.1016/S1875-5372(10)60100-2

[2] Moussaoui, Kamel, Walter Rubio, Michel Mousseigne, Tarek Sultan, and F. Rezai. "Effects of Selective Laser Melting additive manufacturing parameters of Inconel 718 on porosity, microstructure and mechanical properties." *Materials Science and Engineering: A* 735 (2018): 182-190. https://doi.org/10.1016/j.msea.2018.08.037

[3] Royer, Alexandre, Thierry Barriere, and Yves Bienvenu. "Influence of supercritical debinding and processing parameters on final properties of injection-moulded Inconel 718." *Powder technology* 336 (2018): 311-317. https://doi.org/10.1016/j.powtec.2018.05.047

[4] Dugauguez, Olivier, José Manuel Torralba, Thierry Barriere, and Jean-Claude Gelin. "Unconventional methods of sintering Inconel 718 MIM samples." *Powder Metallurgy* 60, no. 2 (2017): 131-138. https://doi.org/10.1080/00325899.2016.1270389
[5] Jia, Qingbo, and Dongdong Gu. "Selective laser melting additive manufacturing of Inconel 718 superalloy parts: Densification, microstructure and properties." *Journal of Alloys and Compounds* 585 (2014): 713-721. https://doi.org/10.1016/j.jallcom.2013.09.171
[6] Caminero, Miguel Ángel, Ana Romero Gutiérrez, Jesús Miguel Chacón, Eustaquio García-Plaza, and Pedro José Núñez. "Effects of fused filament fabrication parameters on the manufacturing of 316L stainless-steel components: geometric and mechanical properties." *Rapid Prototyping Journal* 28, no. 10 (2022): 2004-2026. https://doi.org/10.1108/RPJ-01-2022-0023
[7] Mousapour, Mehrdad, Mika Salmi, Lassi Klemettinen, and Jouni Partanen. "Feasibility study of producing multi-metal parts by Fused Filament Fabrication (FFF) technique." *Journal of Manufacturing Processes* 67 (2021): 438-446.
[8] Roshchupkin, Stanislav, Alexander Kolesov, Alexey Tarakhovskiy, and Ivan Tishchenko. "A brief review of main ideas of metal fused filament fabrication." *Materials Today: Proceedings* 38 (2021): 2063-2067. https://doi.org/10.1016/j.matpr.2020.10.142
[9] Tosto, Claudio, Jacopo Tirillò, Fabrizio Sarasini, and Gianluca Cicala. "Hybrid metal/polymer filaments for fused filament fabrication (FFF) to print metal parts." *Applied Sciences* 11, no. 4 (2021): 1444. https://doi.org/10.3390/app11041444
[10] Damon, James, Stefan Dietrich, Sasidhar Gorantla, Uwe Popp, Brando Okolo, and Volker Schulze. "Process porosity and mechanical performance of fused filament fabricated 316L stainless steel." *Rapid Prototyping Journal* 25, no. 7 (2019): 1319-1327. https://doi.org/10.1108/RPJ-01-2019-0002
[11] Singh, Sunpreet, Gurminder Singh, Chander Prakash, and Seeram Ramakrishna. "Current status and future directions of fused filament fabrication." *Journal of Manufacturing Processes* 55 (2020): 288-306. https://doi.org/10.1016/j.jmapro.2020.04.049
[12] Godec, Damir, Santiago Cano, Clemens Holzer, and Joamin Gonzalez-Gutierrez. "Optimization of the 3D printing parameters for tensile properties of specimens produced by fused filament fabrication of 17-4PH stainless steel." *Materials* 13, no. 3 (2020): 774. https://doi.org/10.3390/ma13030774
[13] Jimbo, Koki, and Toshitake Tateno. "Shape contraction in sintering of 3D objects fabricated via metal material extrusion in additive manufacturing." *International Journal of Automation Technology* 13, no. 3 (2019): 354-360. https://doi.org/10.20965/ijat.2019.p0354
[14] Nurhudan, Aghnia Ilmiah, Sugeng Supriadi, Yudan Whulanza, and Agung Shamsuddin Saragih. "Additive manufacturing of metallic based on extrusion process: A review." *Journal of Manufacturing Processes* 66 (2021): 228-237. https://doi.org/10.1016/j.jmapro.2021.04.018
[15] Sadaf, M., M. Bragaglia, and F. Nanni. "A simple route for additive manufacturing of 316L stainless steel via Fused Filament Fabrication." *Journal of Manufacturing Processes* 67 (2021): 141-150. https://doi.org/10.1016/j.jmapro.2021.04.055
[16] Liu, Bin, Yuxiang Wang, Ziwei Lin, and Tao Zhang. "Creating metal parts by fused deposition modeling and sintering." *Materials Letters* 263 (2020): 127252. https://doi.org/10.1016/j.matlet.2019.127252
[17] Thompson, Yvonne, Kai Zissel, Andreas Förner, Joamin Gonzalez-Gutierrez, Christian Kukla, Steffen Neumeier, and Peter Felfer. "Metal fused filament fabrication of the nickel-base superalloy IN 718." *Journal of Materials Science* 57, no. 21 (2022): 9541-9555. https://doi.org/10.1007/s10853-022-06937-y
[18] Thompson, Yvonne, Joamin Gonzalez-Gutierrez, Christian Kukla, and Peter Felfer. "Fused filament fabrication, debinding and sintering as a low cost additive manufacturing method of 316L stainless steel." *Additive Manufacturing* 30 (2019): 100861. https://doi.org/10.1016/j.addma.2019.100861
[19] Zhang, Yaozhong, Shengyuan Bai, Mirko Riede, Elias Garratt, and Aljoscha Roch. "A comprehensive study on fused filament fabrication of Ti-6Al-4V structures." *Additive Manufacturing* 34 (2020): 101256. https://doi.org/10.1016/j.addma.2020.101256
[20] Wang, Yun, Li Zhang, Xun Li, and Zhao Yan. "On hot isostatic pressing sintering of fused filament fabricated 316L stainless steel–evaluation of microstructure, porosity, and tensile properties." *Materials Letters* 296 (2021): 129854. https://doi.org/10.1016/j.matlet.2021.129854
[21] Santamaria, Ricardo, Mobin Salasi, Sam Bakhtiari, Garry Leadbeater, Mariano Iannuzzi, and Md Zakaria Quadir. "Microstructure and mechanical behaviour of 316L stainless steel produced using sinter-based extrusion additive manufacturing." *Journal of Materials Science* (2022): 1-17. https://doi.org/10.1007/s10853-021-06828-8
[22] Gonzalez-Gutierez, J., Damir Godec, R. Guráň, Martin Spörk, Christian Kukla, and Clemens Holzer. "3D printing conditions determination for feedstock used in fused filament fabrication (FFF) of 17-4PH stainless steel parts." *Metalurgija* 57, no. 1-2 (2018): 117-120.

[23] Zhang, Qiang, Pan Ren, Xiaohui Tu, Yuhong Dai, Xiaojian Wang, and Wei Li. "Effect of heat treatment on microstructure evolution and mechanical properties of selective laser melted Inconel 718 alloy." *Journal of Materials Engineering and Performance* 28 (2019): 5376-5386. https://doi.org/10.1007/s11665-019-04309-3

[24] Buckman, Jim, Shereef A. Bankole, Stephanie Zihms, Helen Lewis, Gary Couples, and Patrick WM Corbett. "Quantifying porosity through automated image collection and batch image processing: case study of three carbonates and an aragonite cemented sandstone." *Geosciences* 7, no. 3 (2017): 70. https://doi.org/10.3390/geosciences7030070

[25] Mostafaei, Amir, Pierangeli Rodriguez De Vecchis, Ian Nettleship, and Markus Chmielus. "Effect of powder size distribution on densification and microstructural evolution of binder-jet 3D-printed alloy 625." *Materials & Design* 162 (2019): 375-383. https://doi.org/10.1016/j.matdes.2018.11.051

[26] Ammosova, Lena, Santiago Cano Cano, Stephan Schuschnigg, Christian Kukla, Kari Mönkkönen, Mika Suvanto, and Joamin Gonzalez-Gutierrez. "Effect of metal particle size and powder volume fraction on the filling performance of powder injection moulded parts with a microtextured surface." *Precision Engineering* 72 (2021): 604-612. https://doi.org/10.1016/j.precisioneng.2021.06.014

[27] Choi, Joon-Phil, Gi-Hun Shin, Sangsun Yang, Dong-Yeol Yang, Jai-Sung Lee, Mathieu Brochu, and Ji-Hun Yu. "Densification and microstructural investigation of Inconel 718 parts fabricated by selective laser melting." *Powder Technology* 310 (2017): 60-66. https://doi.org/10.1016/j.powtec.2017.01.030

[28] Cherry, J. A., H. M. Davies, S. Mehmood, N. P. Lavery, S. G. R. Brown, and JJTIJoAMT Sienz. "Investigation into the effect of process parameters on microstructural and physical properties of 316L stainless steel parts by selective laser melting." *The International Journal of Advanced Manufacturing Technology* 76 (2015): 869-879. https://doi.org/10.1007/s00170-014-6297-2